Effects of deformations and orientations in the fission of the actinide nuclear system ^{254}Fm* formed in the ^{11}B + ^{243}Am reaction

Manpreet Kaur,[1] Manoj K. Sharma,[1] and Raj K. Gupta[2]
[1]*School of Physics and Materials Science, Thapar University, Patiala 147004, India*
[2]*Department of Physics, Panjab University, Chandigarh 160014, India*
(Received 12 July 2012; published 26 December 2012)

We have studied the decay of actinide nuclear system ^{254}Fm* formed in ^{11}B + ^{243}Am reaction using the dynamical cluster decay model (DCM), with choices of spherical, quadrupole deformation β_2 alone and higher multipole deformations β_2–β_4. For β_2 deformations, the optimum orientations $\theta_i^{\rm opt}$ are used whereas for higher multipole deformations the compact orientations θ_i^c of decaying fragments are taken in to account. Besides static-β_2 deformations, the effects of dynamical-β_2 deformations are also explored. The calculated cross sections find excellent agreement with the available experimental data with spherical as well as deformed choices of fragmentations, enabling us to account for the role of important nuclear deformation effects in the ^{11}B-induced nuclear reaction. Spontaneous decay of ^{254}Fm with cold elongated configuration and optimum orientation is also worked out. The mass distributions of excited fermium isotopes in the neighborhood of ^{254}Fm* are also explored. In addition, the roles of temperature, angular momentum, and fission fragment anisotropies are investigated in the context of the chosen reaction.

DOI: 10.1103/PhysRevC.86.064610 PACS number(s): 25.70.Jj, 24.10.−i, 25.85.−w, 27.90.+b

I. INTRODUCTION

Heavy-ion-induced reactions are appropriate to explore the dynamics of fusion-fission and related nuclear phenomena. The factors on which the fusion-fission dynamics depend are still not fully understood. Some of them are the large Coulomb repulsion, the entrance channel mass asymmetry, and deformations and orientations of projectile (P) and target (T). The reactions having large Coulomb repulsion may fail to form a compound nucleus even if the system overcomes the fusion barrier. This is because the distance between the centers of projectile and target at the contact point is larger than that of nascent fragments at the saddle point [1]. However, the same is not true for the light projectile-target combinations, as the difference in the sizes of projectile and target is quite large. According to the pre-equilibrium fission model [2,3], the mass asymmetry [$\alpha = (A_T - A_P)/(A_T + A_P)$] is another quantity that plays an important role in deciding the contribution from non-compound-nucleus (nCN) fission. In the context of this model if the entrance-channel mass asymmetry $\alpha > \alpha_{\rm BG}$, the Businaro-Gallone (BG) mass asymmetry [4], then nCN is not expected. However, for $\alpha < \alpha_{\rm BG}$ the nCN contribution is not ruled out. In the entrance-channel-dependent (ECD) K-state model of Vorkapic and Ivanisevic [5], target deformation plays an important role in deciding the contribution from nCN fission. When the projectile collides with the tip of the deformed target, compound nucleus formation takes place only if the composite system lies within the saddle point; otherwise the compound system is elongated enough that it may escape into the exit channel without being captured within the saddle point to form the compound nucleus, resulting in nCN fission contribution.

Recently, the reaction ^{11}B + ^{243}Am has been studied experimentally [6], and its mass asymmetry $\alpha > \alpha_{\rm BG}$ suggests that the nCN contribution should be absent on the basis of the pre-equilibrium fission model [2,3]. However, the observed fission fragment anisotropies are anomalous with regard to the statistical model values [6], and hence the presence of nCN contribution is anticipated. According to the authors of this paper [6], the mass asymmetry alone is not enough to decide the nCN contribution and, following the ECD K-state model [5], the target deformation should play an important role in fixing the anomalous behavior of fission fragment anisotropies. In this paper, we have addressed this question of the role of target deformation and other aspects of deformations and orientations of related fission fragments of ^{254}Fm* nucleus on the basis of the dynamical cluster-decay model (DCM) [7–19]. In the reaction under study, the target nucleus ^{243}Am has a static quadrupole deformation $\beta_2 = 0.224$, taken from Ref. [20]. The compound nucleus ^{254}Fm* is also deformed ($\beta_2 = 0.237$), which helps to proceed on its fission path. In DCM, the static deformations and orientation degrees of freedom of one or both decay fragments are expected to influence the fusion-fission probability. We have also used the dynamically induced deformations since the fusion cross sections are also expected to differ depending upon whether the deformation is static or dynamically induced [21].

Within the DCM, the decay of actinide nuclear system ^{254}Fm* formed in the ^{11}B + ^{243}Am reaction over a range of energies ($E_{\rm lab} = 60$–72 MeV) [6] is studied by taking the decay fragments of either spherical or with quadrupole deformations (β_2) and optimum orientation ($\theta_i^{\rm opt}$) [10] and higher multipole deformations up to hexadecapole (β_2–β_4) with compact orientations (θ_i^c) [22]. The DCM calculated cross sections are in reference to experimental data of Ref. [6]. ^{254}Fm* is a fissile nucleus imparting negligible contribution to evaporation residue. The spontaneous decay of fermium is also investigated for comparing the mass distribution of the decay of ^{254}Fm in hot (temperature $T \neq 0$) and cold ($T = 0$) fusion-fission processes. Because ^{254}Fm is a neutron-rich actinide nuclear system with $Z = 100$, it also decays spontaneously [23] with an asymmetric mass distribution, also

studied earlier within the quantum mechanical fragmention theory [24], which provides a basis for DCM also. The mass distributions of various isotopes ^{250,252,256,258}Fm* are also worked out at $E_{\rm lab} = 60$ MeV within DCM. Also, the fission fragment anisotropies are calculated within the standard saddle-point statistical model (SSPM) [25] approach using the DCM-based parameters.

The paper is organized as follows: The DCM for a hot and rotating compound system is discussed briefly in Sec. II. The calculations and results obtained for the decay of ^{254}Fm* nucleus are discussed in Sec. III. Finally, a summary of our results is given in Sec. IV.

II. THE DYNAMICAL CLUSTER-DECAY MODEL (DCM)

The DCM is used for a variety of compound-nucleus-based nuclear reactions [7–19]. Its basis is the well-known quantum mechanical fragmentation theory (see, e.g., Refs. [26–28]), which is worked out in terms of the collective coordinates of the mass asymmetry $\eta = \frac{A_1-A_2}{A_1+A_2}$ and charge asymmetry $\eta_Z = \frac{Z_1-Z_2}{Z_1+Z_2}$ (1 and 2 stand, respectively, for heavy and light fragments) and the relative separation R. The multipole deformations $\beta_{\lambda i}$ ($\lambda = 2,\ 3,\ 4$; $i = 1,\ 2$) and orientations θ_i of two nuclei or fragments are included via the radius vectors R_i, defined later. In terms of these coordinates, using ℓ partial waves, the compound nucleus decay or the fragment production cross section is given by

$$\sigma = \sum_{\ell=0}^{\ell_{\max}} \sigma_\ell = \frac{\pi}{k^2} \sum_{\ell=0}^{\ell_{\max}} (2\ell+1) P_0 P; \quad k = \sqrt{\frac{2\mu E_{\rm c.m.}}{\hbar^2}}, \tag{1}$$

where the preformation probability P_0 refers to η motion and the penetrability P to R motion. Here the compound nucleus is considered to be formed with a probability equal to one (an assumption more suitable for higher energies but extended here also to lower energies) and, in general, independent of the incoming channel. However, the entrance-channel effects in DCM enter via the maximum angular momentum $\ell_{\max}$ or its critical value $\ell_{\rm crit}$ which depends on the entrance-channel mass asymmetry η_{in} [29]. $\mu = [A_1A_2/(A_1+A_2)]m = \frac{1}{4}A_{\rm CN}m(1-\eta^2)$ is the reduced mass and $\ell_{\max}$ is the maximum angular momentum, defined for light-particles (LP) cross section $\sigma_{\rm LP} \to 0$. m is the nucleon mass. Equation (1) is also used for the noncompound nucleus, quasifission process, where the incoming channel does not loose its identity, and hence $P_0 = 1$ for quasifission.

In Eq. (1), the preformation probability P_0 is given by the solution of the stationary Schrödinger equation in η, at fixed $R = R_a$,

$$\left\{ -\frac{\hbar^2}{2\sqrt{B_{\eta\eta}}} \frac{\partial}{\partial\eta} \frac{1}{\sqrt{B_{\eta\eta}}} \frac{\partial}{\partial\eta} + V(\eta, R, T) \right\} \psi^\nu(\eta) = E^\nu \psi^\nu(\eta), \tag{2}$$

with $\nu = 0,\ 1,\ 2,\ 3,\ \ldots$ referring to ground-state ($\nu = 0$) and excited-state solutions, with the ground-state P_0 given as

$$P_0 = |\psi^{\nu=0}[\eta(A_i)]|^2 \sqrt{B_{\eta\eta}} \frac{2}{A_{\rm CN}}. \tag{3}$$

The mass parameters $B_{\eta\eta}(\eta)$, used in the calculations of P_0, representing the kinetic energy term, are the smooth classical hydrodynamical masses [30]. It is worth mentioning here that at large temperatures (T), the shell effects are not very important and hence smooth classical hydrodynamical masses are used for simplicity. However, for explicit role of shell effects in the inertia parameter $B_{\eta\eta}(\eta)$, one may use shell-corrected masses like cranking masses as explained in Refs. [31,32]. Evidently, P_0 contains the structure information of the compound nucleus, which enters Eq. (2) via the fragmentation potential,

$$\begin{aligned} V(\eta, R, T) &= \sum_{i=1}^{2} [V_{\rm LDM}(A_i, Z_i, T)] + \sum_{i=1}^{2} [\delta U_i] \exp\left(-T^2/T_0^2\right) \\ &\quad + V_C(R, Z_i, \beta_{\lambda i}, \theta_i, T) + V_P(R, A_i, \beta_{\lambda i}, \theta_i, T) \\ &\quad + V_\ell(R, A_i, \beta_{\lambda i}, \theta_i, T). \end{aligned} \tag{4}$$

$V_{\rm LDM}$ in the above equation is T-dependent liquid drop energy of Davidson *et al.* [33] and δU, the "empirical" shell correction from Myers and Swiatecki [34], is also made T dependent to vanish exponentially with $T_0 = 1.5$ MeV [35]. V_C, V_P, and V_ℓ are, respectively, the T-dependent Coulomb, the nuclear proximity [36], and the centrifugal potentials, with the moment of inertia taken in the complete sticking limit. The deformation effects are incorporated in Coulomb potential, which is given as

$$\begin{aligned} V_C(R, Z_i, \beta_{\lambda i}, \theta_i, T) &= Z_1Z_2e^2/R(T) + 3Z_1Z_2e^2 \sum_{\lambda, i=1,2} \frac{R_i^\lambda(\alpha_i, T)}{(2\lambda+1)R(T)^{\lambda+1}} \\ &\quad \times Y_\lambda^{(0)}(\theta_i) \left[\beta_{\lambda i} + \frac{4}{7}\beta_{\lambda i}^2 Y_\lambda^{(0)}(\theta_i) \right] \end{aligned} \tag{5}$$

with $Y_\lambda^{(0)}(\theta_i)$ as the spherical harmonics function. The centrifugal potential is given by

$$V_\ell(R, A_i, \beta_{\lambda i}, \theta_i, T) = \frac{\hbar^2 \ell(\ell+1)}{2I(T)} \tag{6}$$

with $I = I_S = \mu R^2 + \frac{2}{5}A_1 m R_1^2(\alpha_1, T) + \frac{2}{5}A_2 m R_2^2(\alpha_2, T)$, the moment of inertia in the sticking limit, or, alternatively, the one calculated in nonsticking (NS) limit, $I = I_{\rm NS} = \mu R^2$.

The static deformations $\beta_{\lambda i}$, taken from Ref. [20], are made temperature dependent for quadrupole deformation through the relation [37,38]

$$\beta_2(T) = \beta_2(0) e^{-T/T_0}, \tag{7}$$

where $T_0 = 1.5$ MeV. This temperature dependence of β_2 is consistent with experiments at zero temperature [39].

For the decay of a hot compound nucleus (CN), R_a is the first turning point of the penetration path(s), used for calculating the penetrability P, shown in Fig. 1 for the illustrative case of symmetric fission of ^{254}Fm* for spherical as

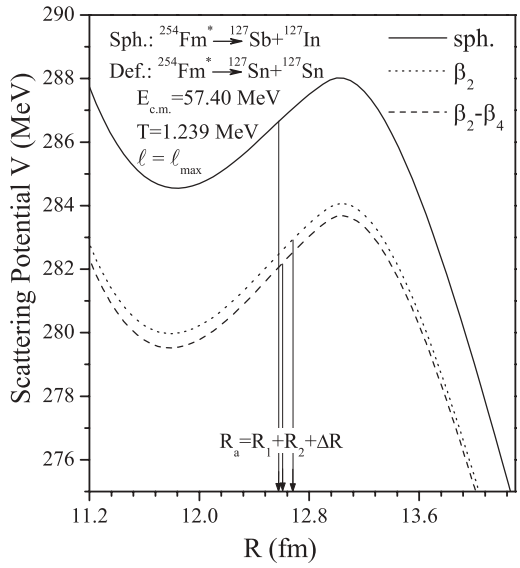

FIG. 1. Scattering potentials $V(R, \ell)$ as a function of R for fixed ℓ, for the decay $^{254}Fm^{*} \rightarrow ^{127}Sb + ^{127}In$ for the spherical and $^{254}Fm^{*} \rightarrow ^{127}Sn + ^{127}Sn$ for the deformed (β_2 and β_2–β_4) choices of fragmentations at $E_{c.m.} = 57.40$ MeV.

well as for β_2 and (β_2–β_4) deformed choices of fragmentation,

$$R_a = R_1(\alpha_1, T) + R_2(\alpha_2, T) + \Delta R(T) = R_t(\alpha, T) + \Delta R(T) \quad (8)$$

with radius vectors

$$R_i(\alpha_i, T) = R_{0i}(T)\left[1 + \sum_{\lambda} \beta_{\lambda i} Y_{\lambda}^{(0)}(\alpha_i)\right]. \quad (9)$$

$\Delta R(T)$ is the only fitting parameter of the model and determines the first turning point of barrier penetration, referring to the barrier height actually used. In terms of two-center shell model, $\Delta R(T)$ assimilates the neck-formation effects [40–42] and is therefore called neck length parameter. In terms of R_a, ΔR is the relative separation between two fragments, similar to that used in scission-point [43] and saddle-point [44,45] statistical fission models. It takes care of the penetration point through the potential barrier. The parameter ΔR, referring to the potential $V(R_a, \ell)$ at $R = R_a$ for each ℓ, can also be related in a simple way to the top of the barrier $V_B(\ell)$ by defining their difference $\Delta V_B(\ell)$ as the effective lowering of the barrier. This barrier modification $\Delta V_B(\ell)$ is therefore a built-in feature of DCM, because of which it can handle the problems related to fusion hindrance and fusion enhancement across the barrier. ΔV_B, which relates $V(R_a, \ell)$ and $V_B(\ell)$, for each ℓ, is defined as

$$\Delta V_B(\ell) = V(R_a, \ell) - V_B(\ell). \quad (10)$$

Here $V(R_a, \ell)$ represents the actual barrier used for the penetration.

The T-dependent nuclear radii R_{0i} of the equivalent spherical nuclei [46] are given as

$$R_{0i}(T) = \left[1.28A_i^{1/3} - 0.76 + 0.8A_i^{-1/3}\right](1 + 0.0007T^2). \quad (11)$$

The compound nucleus temperature T (in MeV) is given by

$$E^*_{CN} = aT^2 - T, \quad (12)$$

with the level density parameter $a = A_{CN}/9$ used here. It may be noted here that the shape of the composite system, the radius vector, depends on the temperature T where the shape parameter β is considered to be both of static (ground-state) value [20] and T dependent [Eq. (7)].

The penetrability P in Eq. (1) is the Wentzel-Kramers-Brillouin (WKB) integral between R_a and R_b,

$$P = \exp\left[-\frac{2}{\hbar}\int_{R_a}^{R_b}\{2\mu[V(R) - Q_{\rm eff}]\}^{1/2} dR\right], \quad (13)$$

solved analytically [8], with R_b as the second turning point satisfying

$$V(R_a, \ell) = V(R_b, \ell) = Q_{\rm eff}(T, \ell) = E_{\rm kin}(T), \quad (14)$$

where $Q_{\rm eff}$ denotes the effective Q value in WKB intergral and $E_{\rm kin}$ is the total kinetic energy. For details, see Ref. [9].

Within the SSPM approach [25], the fission fragment anisotropy A is related to the total ℓ value (equivalently $\ell_{\rm max}$) of CN, the effective moment of inertia $I_{\rm eff}$ of the fissioning nucleus in the transition state, and the temperature T at the saddle point, as given by

$$A = 1 + \langle \ell^2 \rangle / 4K_0^2, \quad (15)$$

where $K_0^2 = T \times I_{\rm eff}/\hbar^2$ and $I_{\rm eff}$ is calculated by using the finite-range rotating liquid drop model [47]. We have also calculated the fission fragment anisotropy A, using T as the temperature of the fissioning nucleus, and the $\ell_{\rm max}$ value within nonsticking limit for moment of inertia ($I_{\rm NS}$) in the ℓ-dependent potential V_ℓ.

III. CALCULATIONS

We have made a comparative study of the fragmentation paths of $^{254}Fm^{*}$, using the spherical, the only-β_2 deformed, and the β_2–β_4 deformed cases, over a wide range of available incident energies [6]. Also, a comparison of static-β_2 with dynamic-β_2 deformation is worked out. The DCM-based calculations confirm that $^{254}Fm^{*}$ decays mainly via the fission path and the predicted ER cross sections are negligibly small. Besides this, the issues related to spontaneous fission, isotopic dependence, angular momentum, temperature, and fission fragment anisotropies are also explored.

First of all, we look at the behavior of potential energy surfaces calculated on DCM for the three possible fragmentation paths: (i) spherical, (ii) β_2 static with optimum orientations ($\theta_i^{\rm opt}$), and (iii) higher multipole static deformations (β_2–β_4) with compact orientation (θ_i^c) in the decay of actinide compound nucleus $^{254}Fm^{*}$ formed in $^{11}B + ^{243}Am$ reaction. Figures 2(a) and 2(b) illustrate the fragmentation potentials as a function of fragment mass A_2 for $\ell = 0$ and $\ell = \ell_{\rm max}$ values for these three cases. The optimum orientations $\theta_i^{\rm opt}$ are uniquely fixed on the basis of the quadrupole deformation alone of nuclei [10], and compact orientations θ_i^c for higher multipole deformations (β_2–β_4) are calculated as per prescription in Ref. [22], using hot configurations in both cases. Figures 2(a) and 2(b) show that the potential surfaces

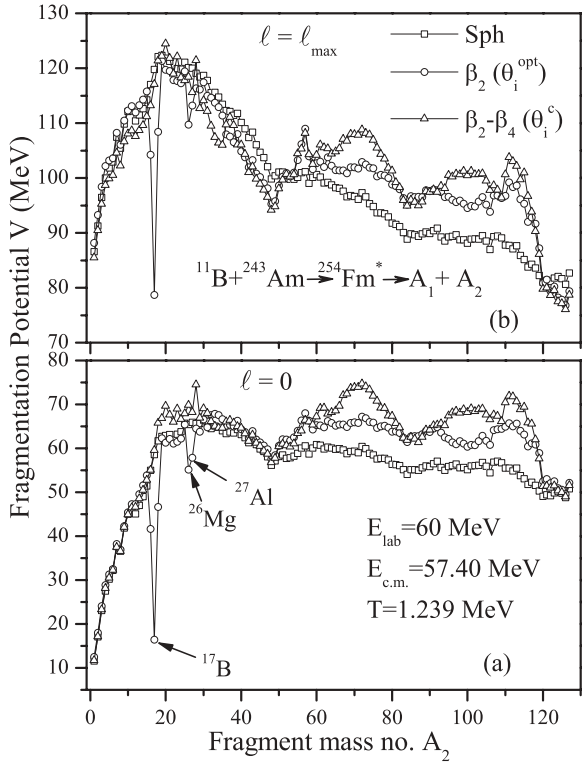

FIG. 2. Fragmentation potential as a function of light mass fragment A_2 for the decay of ^{254}Fm* formed in ^{11}B + ^{243}Am reaction channel for spherical as well as deformed considerations at (a) $\ell = 0$ and (b) $\ell = \ell_{max}$.

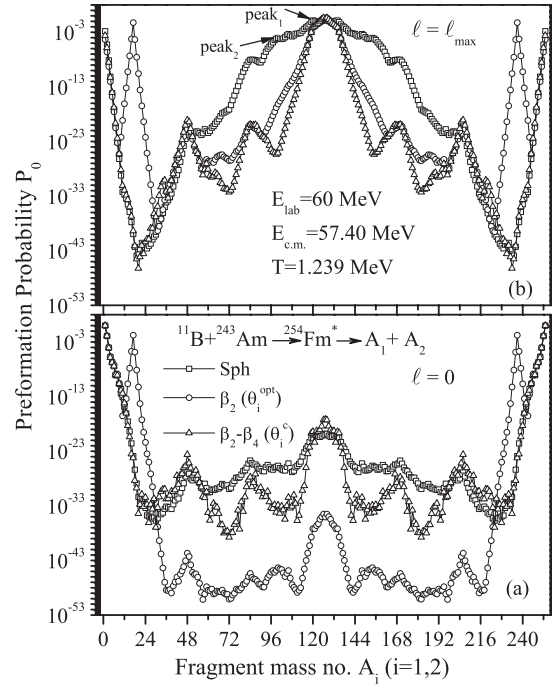

FIG. 3. Same as for Fig. 2, but for the preformation probability P_0 as a function of fragment mass A_i ($i = 1, 2$).

are nearly smooth for the spherical choice of fragmentations at $\ell = 0$ and $\ell = \ell_{max}$, which show enough structure with the inclusion of deformations, and certain minima (^{17}B, ^{26}Mg, ^{27}Al) are observed to be rather deep for the β_2 (static) deformations with optimum orientations. However, these deeper minima do not make any significant contributions since the penetration probability of these fragments is negligibly small. The emergence of these unexpected minima may be due to the inappropriate values of optimized β_2 deformations used in the calculations and occur mainly because of the proximity (V_P) part of the fragmentation potential. We further notice that at $\ell = 0$, the light fragments (representing ER) are more dominant, whereas with the increase in ℓ value the fission fragments start appearing such that at $\ell = \ell_{max}$ value the symmetric fission dominates the ER channel. This aspect is further explored in Fig. 3, showing the preformation probability P_0, obtained by solving the stationary Schrödinger equation (2) in η coordinate.

Figure 3 clearly shows that the decay of ^{254}Fm* follows a symmetric pattern, independent of the deformation effects, though a shoulder structure is seen in the spherical considerations, a signature of asymmetric fission fragments, which vanishes with the addition of deformation effects. We note, however, that the contribution of fragments forming the shoulder is very small. This is depicted in Fig. 4, which shows the asymmetric to symmetric peak ratio ($\frac{\text{Peak}_2}{\text{Peak}_1}$) as a function of $E_{\text{c.m.}}$. Peak$_2$ represents the fragments with mass number $A_2 =$ 98–114 and Peak$_1$ represents masses $A_2 = 115$–127. It is clear from Fig. 4 that the contribution of Peak$_2$ is very small. It is approximately 0.6% at the lowest energy and increases to a maximum of 2% at the highest energy. This implies that the contribution of the asymmetric fragments even for spherical choice of fragmentation is negligibly small. One may conclude here that the symmetric fragmentation is preferred in the decay of ^{254}Fm*, independent of spherical, only-β_2, or (β_2–β_4) deformations.

Next, the fission cross sections are calculated, in reference to experimental data of Ref. [6], within the DCM by fitting the only parameter of the model, the neck-length parameter ΔR,

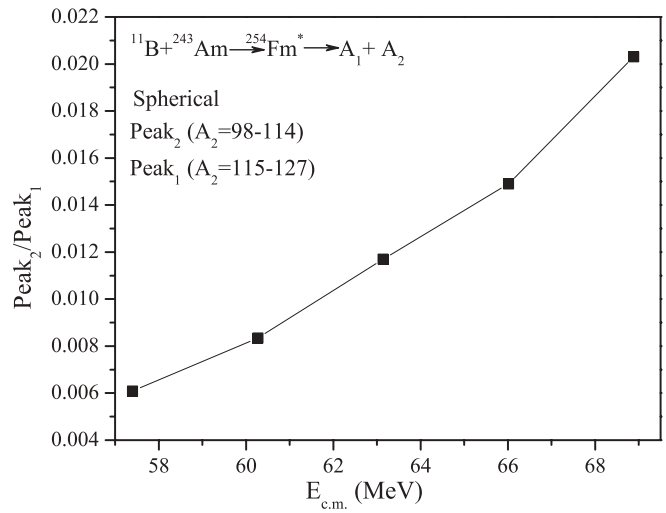

FIG. 4. The ratio of the asymmetric to symmetric fission yields (P_0) as a function of $E_{\text{c.m.}}$ for the spherical choice of nuclei in the fragmentation process of the decay of ^{254}Fm*.

TABLE I. DCM calculated fission cross sections ($\sigma_{\rm fission}$), compared with experimental data [6] and the predicted ER cross sections ($\sigma_{\rm ER}$), for the decay of ^{254}Fm* formed in ^{11}B + ^{243}Am reaction, considering spherical as well as deformed choice of fragments.

$E_{\rm lab}$	$E_{\rm c.m.}$	T	$\Delta R_{\rm fission}$			$\sigma_{\rm fission}$(DCM)			$\sigma_{\rm fission}$	$\sigma_{\rm ER}$ (DCM) at $\Delta R_{\rm fission}$		
(MeV)	(MeV)	(MeV)	sph (fm)	β_2 (fm)	β_2–β_4 (fm)	sph (mb)	β_2 (mb)	β_2–β_4 (mb)	(expt.) (mb)	sph (mb)	β_2 (mb)	β_2-β_4 (mb)
60	57.40	1.239	0.9	1.0025	0.929	175.4	175.6	173.4	176.86	3.37×10^{-7}	1.86×10^{-7}	5.56×10^{-7}
63	60.27	1.28	1.0	1.038	0.986	354	356	352	357.96	5.12×10^{-6}	2.47×10^{-6}	3.13×10^{-6}
66	63.142	1.32	1.042	1.0575	1.017	452	450	450	453.41	1.59×10^{-5}	9.22×10^{-6}	7.96×10^{-6}
69	66.012	1.359	1.0589	1.076	1.0618	610	608	606	609.27	2.69×10^{-5}	2.25×10^{-5}	2.72×10^{-5}
72	68.882	1.396	1.074	1.088	1.0775	710	708	710	709.87	4.42×10^{-5}	3.96×10^{-5}	4.78×10^{-5}

which varies as a function of center of mass (c.m.) energy. We find that for each c.m. energy, the fits can be achieved by the spherical and deformed considerations within the single neck-length parameter ΔR. Figure 5 and Table I show that the DCM calculated fission cross sections are in excellent agreement with the experimental data for all three cases. It is further clear from Table I that the decay is a pure fission decay, with the almost negligible evaporation residue (ER) cross sections calculated at the fission fitted ΔR values. Figure 6 shows the variation of ΔR with $E_{\rm c.m.}$ for the three choices of fragment shapes. We notice that ΔR increases with increase in energy, and that it has higher values for the β_2 deformations, compared to both spherical and β_4 deformations.

Another quantity of interest, related to ΔR, is the variation of barrier-lowering parameter ΔV_B as a function of $E_{\rm c.m.}$, an important property at near- and sub-barrier energies [48]. Figure 7 shows that ΔV_B is the largest for the case of β_2–β_4 at near-barrier energies. On the other hand, at above-barrier energies, the barrier modification is small and comparable for the three cases.

Figure 8 shows the role of dynamic-β_2 compared with static-β_2 deformations with optimum orientations, for the preformation probability P_0 as a function of fragment mass A_i ($i = 1, 2$) for the decay of ^{254}Fm*. We notice that the distribution is symmetric for both the choices of β_2 (static and dynamic), although a small shoulder is formed for the dynamic-β_2 choice of fragmentation, similar to what was seen in the case of spherical choice of fragmentation for static β_2 (refer to Fig. 3). It may be noted that the angular momentum $\ell_{\rm max}$ involved here in the reaction dynamics has higher values. This is because of the use of sticking moment of inertia (I_S) in the centrifugal potential (V_ℓ) term. It is relevant to mention here that nonsticking ($I_{\rm NS}$) approximation gives larger centrifugal potential as compared to sticking (I_S), at the same R [11,17]. Therefore, one would expect larger ℓ values for the use of the I_S approach as compared to that for $I_{\rm NS}$. Since we are using proximity interaction in our model, the use of I_S is more appropriate as structure effects due to proximity forces are more visible for the use of sticking choice of moment of inertia. It may be noted that the use of $I_{\rm NS}$ approach in centrifugal potential weakens the (attractive) nuclear proximity interaction and hence $V_\ell(I_S)$ with relatively lower magnitude is preferred.

We have also calculated the fission cross sections with dynamic-β_2 deformations, by fitting again the neck-length parameter ΔR. The two ΔR's are compared in Fig. 9(a),

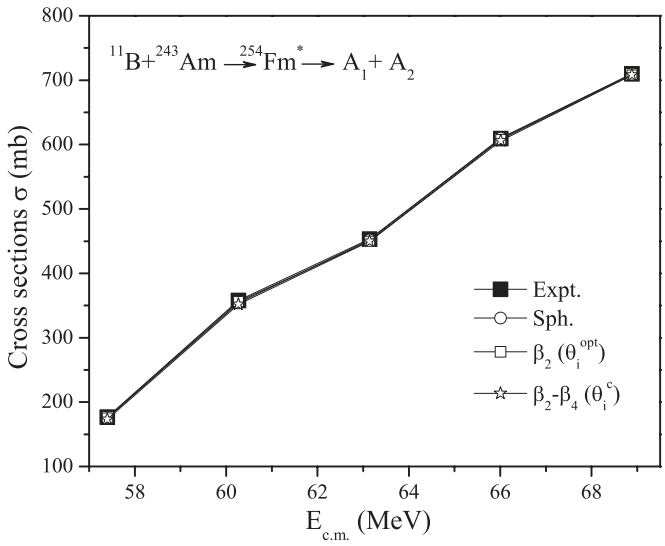

FIG. 5. The DCM calculated fission cross sections, compared with the experimental data [6], for the decay of ^{254}Fm* formed in ^{11}B + ^{243}Am reaction as a function of $E_{\rm c.m.}$ for spherical, only-β_2 deformation, and higher multipole deformations up to hexadecapole (β_2–β_4) choices of the fragmentation process.

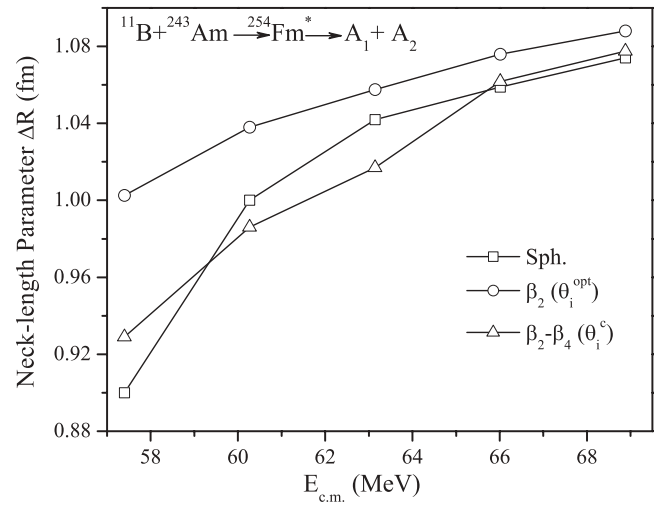

FIG. 6. The fitted neck-length parameter ΔR for fission decay of ^{254}Fm* formed in ^{11}B + ^{243}Am reaction, as function of $E_{\rm c.m.}$, for spherical as well as deformed considerations.

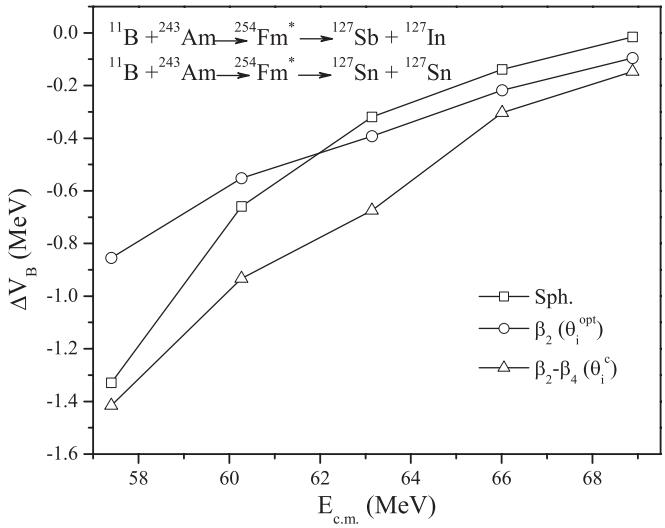

FIG. 7. The barrier-lowering parameter ΔV_B as a function of $E_{\text{c.m.}}$ for the decay $^{254}\text{Fm}^* \rightarrow ^{127}\text{Sb} + ^{127}\text{In}$ for spherical fragments and $^{254}\text{Fm}^* \rightarrow ^{127}\text{Sn} + ^{127}\text{Sn}$ for deformed (β_2 and β_2–β_4) fragments.

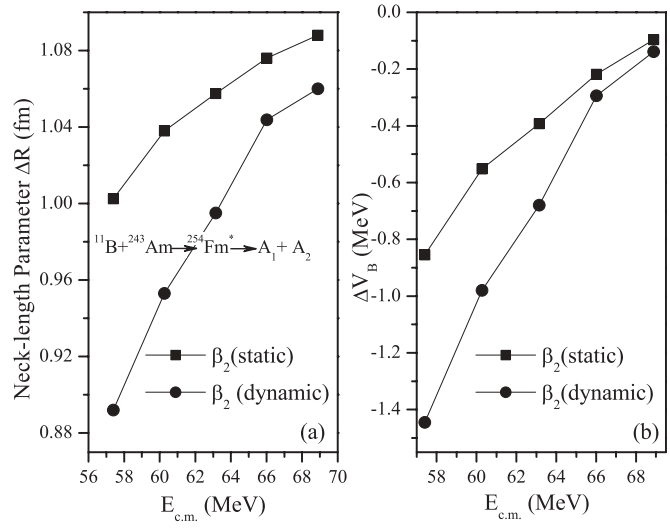

FIG. 9. (a) The fitted neck-length parameter ΔR and (b) the barrier lowering parameter ΔV_B for fission of $^{254}\text{Fm}^*$, as a function of $E_{\text{c.m.}}$, for the β_2-static as well as β_2-dynamic deformations.

showing that the static ΔR values are higher than for dynamic β_2 choice of fragmentations. A similar comparison for ΔV_B values for β_2 static and β_2 dynamic is shown in Fig. 9(b), which clearly depicts that the barrier lowering at near-barrier energies is greater for the β_2-dynamic than for β_2-static choice of fragmentation. At higher energies, however, the difference becomes minimal and ΔV_B goes to zero in both cases.

It is of further interest to look for the fragmentation behavior of the various isotopes of fermium. Figure 10 shows the calculated preformation probability P_0 for various isotopes of fermium ($^{250-258}\text{Fm}^*$) as a function of fragment mass number A_i ($i = 1, 2$). The calculations are made at $E_{\text{lab}} = 60$ MeV by taking the same value for the neck-length parameter ΔR and $\ell_{\max}$ value as for $^{254}\text{Fm}^*$ at the said energy. Only the case of β_2-deformed fragmentation is considered. We notice in Fig. 10 that the decay of fermium isotopes still follows the symmetric distribution when two or four neutrons are added to or subtracted from $^{254}\text{Fm}^*$. Although a small hump is seen for the neutron-deficient $^{250}\text{Fm}^*$, similar to the one observed in the case of spherical fragmentation of $^{254}\text{Fm}^*$, the contribution of this asymmetric hump is again negligibly small.

We have seen from Figs. 3 and 10 that the mass distribution is symmetric for the decay of excited $^{254}\text{Fm}^*$ and its isotopes $^{252,256,258}\text{Fm}^*$ formed in heavy-ion reactions. However, this result may not be valid for the spontaneous ($T = 0$) decay of ^{254}Fm. Figure 11 shows the preformation probability P_0 as a function of fragment mass for the spontaneous decay of ^{254}Fm for cold elongated configuration with β_2-deformed, optimum orientation approach. It is clear from Fig. 11 that the mass distribution is asymmetric for the spontaneous decay, in

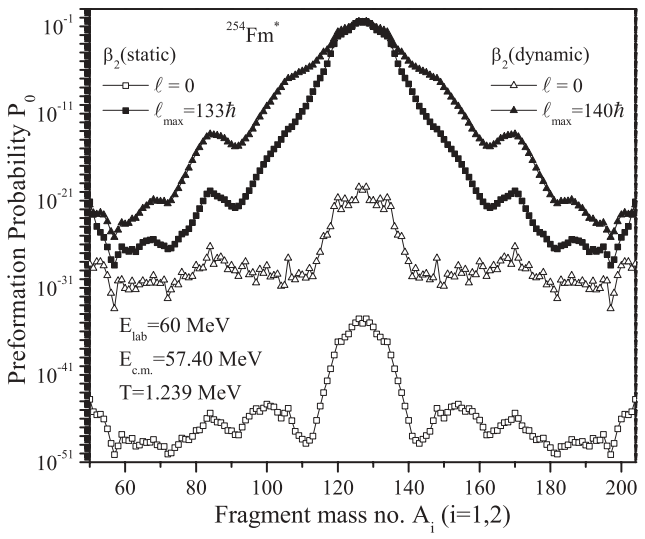

FIG. 8. Preformation probability P_0 as a function of fragment mass number A_i ($i = 1, 2$) for the decay of $^{254}\text{Fm}^*$ formed in $^{11}\text{B} + ^{243}\text{Am}$ reaction channel at $E_{\text{Lab}} = 60$ MeV for β_2-dynamic compared with β_2-static deformations of fragments.

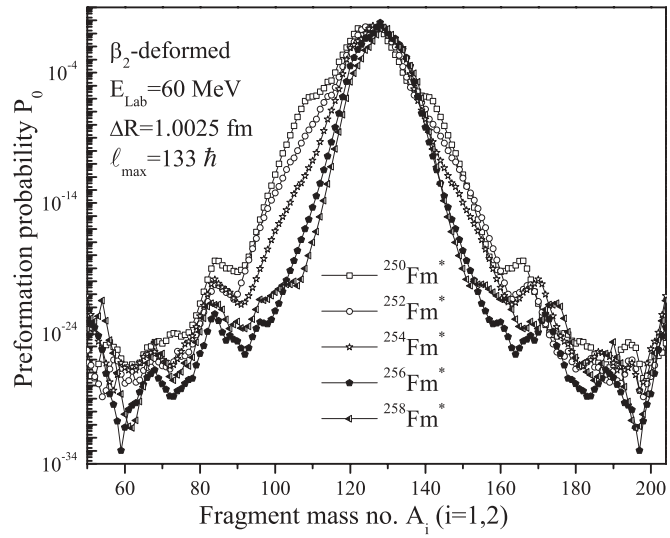

FIG. 10. Preformation probability P_0 as a function of fragment mass number A_i ($i = 1, 2$) for $^{250-258}\text{Fm}^*$ isotopes at $E_{\text{lab}} = 60$ MeV.

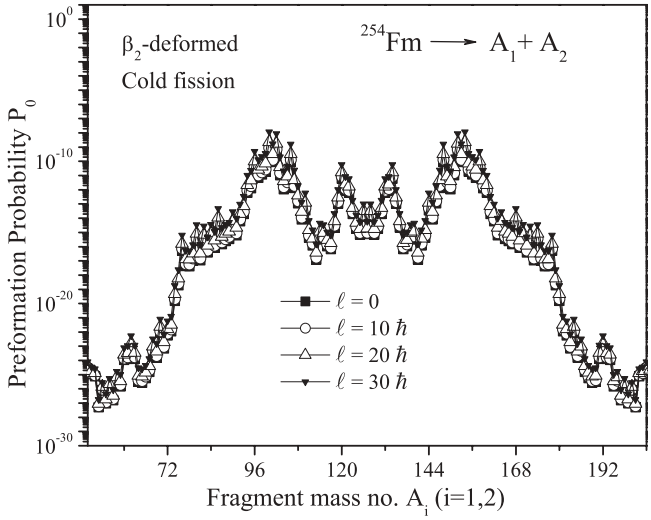

FIG. 11. Preformation probability P_0 as a function of fragment mass number A_i ($i = 1, 2$) for the spontaneous decay (cold fission) of ^{254}Fm using β_2-deformed cold ($T = 0$) elongated configuration at different ℓ values.

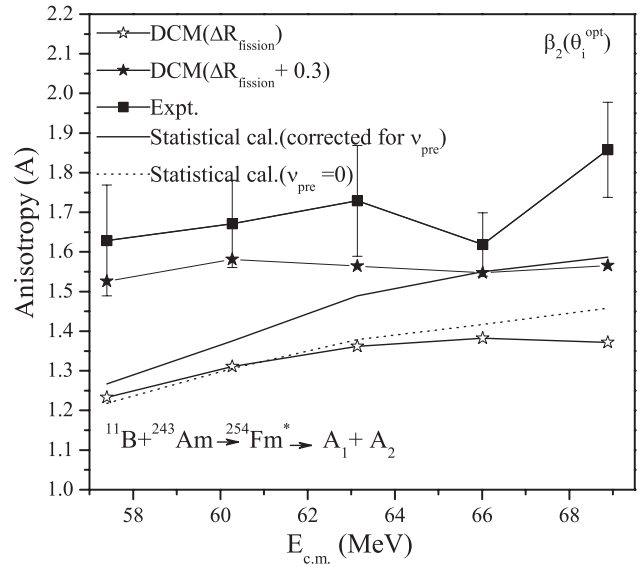

FIG. 12. The DCM calculated fission fragment anisotropies for the case of β_2 deformation in ^{254}Fm*, compared with the experimental data [6] and statistical model calculations (with and without correcting for prefission neutrons).

contrast to being symmetric for the heavy-ion-induced decay in Figs. 3 and 10. One can also observe from Fig. 11 that the angular momentum (ℓ) does not affect the structure of P_0 much. This asymmetric behavior for the spontaneous decay of ^{254}Fm is consistent with a previous calculation and the experiments [24].

Finally, the fission fragment anisotropies are calculated within the SSPM approach using DCM calculated $\ell_{\max}$ values for the nonsticking limit for the moment of inertia ($I_{\rm NS}$) using β_2-deformed consideration. It is relevant to note here that the nonsticking moment-of-inertia limit ($I_{\rm NS}$) is preferred for fission fragment anisotropy calculations and the sticking limit (I_S) for cross sections [17]. In Fig. 12, the DCM calculated fission fragment anisotropies are shown at ΔR values the same as those for fission, which means using the same ΔR as that used for cross-section fitting with the sticking moment-of-inertia limit I_S. Statistical model calculations, with and without ($\nu_{\rm pre} \neq 0$ or $\nu_{\rm pre} = 0$) correction for prefission neutrons, are also given for comparisons. We notice that the DCM-calculated fission fragment anisotropies for $\Delta R_{\rm fission}$ are comparable with the statistical model calculations without correcting for prefission neutrons ($\nu_{\rm pre} = 0$), but not with the experimental data. Knowing that ΔR for $I_{\rm NS}$ is larger than for I_S [17], we have also made calculations increasing the $\Delta R_{\rm fission}$ by 0.3 fm. As expected, for this choice of ΔR, calculated fission fragment anisotropies start approaching the lower limit of experimental values. Apparently, the best fit for $\Delta R_{\rm fission}$ plus a constant or ΔR for $I_{\rm NS}$ could be obtained, but it is not attempted here.

Lastly, we have also attempted to see the contribution of competing non-compound-nucleus (nCN) quasifission (qf) channel in the decay of ^{254}Fm*. The calculations are done by taking $P_0 = 1$ for the incident channel ^{11}B + ^{243}Am since the incoming fragments do not loose their identity in qf process. The DCM-based qf contribution is maximum up to 3% of the fission cross section.

IV. SUMMARY

In this paper, we have calculated the fusion-fission excitation functions of ^{254}Fm* for the ^{11}B + ^{243}Am reaction, using the spherical, only-β_2, and higher multipole (β_2–β_4) deformations with proper compact orientations of fragments. The nice comparison between the DCM calculated and experimental fission cross sections at all energies suggests that the contribution of the competing non-compound-nucleus qf component is quite small, amounting to a maximum of up to 3% of the fission cross section. The comparison of β_2-static and β_2-dynamic deformation is also worked out for the fragmentation path of ^{254}Fm* nucleus. In the case of spontaneous decay of ^{254}Fm, an asymmetric fission is preferred, whereas in the heavy-ion-induced decay of ^{254}Fm*, the mass distribution is clearly symmetric, independent of the deformation effects. The various isotopes of compound nucleus fermium ($^{250-258}$Fm*) also show symmetric behavior in their fragmentation path. The fission fragment anisotropies, calculated at $\Delta R_{\rm fission}$, are in agreement with the statistical model calculations, but for ΔR increased to bring it close to $I_{\rm NS}$ value, the anisotropies start approaching the experimental data. The neck-length parameter ΔR is found to be relatively larger for β_2-deformed case and comparable for spherical and β_2–β_4 deformations. Although the fragmentation behavior is influenced due to the inclusion of deformation effects, the overall fission path remains symmetric for the excited ^{254}Fm* and its neighboring isotopes.

ACKNOWLEDGMENTS

The financial support from the University Grant Commission (UGC), New Delhi, is gratefully acknowledged.

[1] K. Nishio, H. Ikezoe, S. Mitsuoka, K. Satou, and S. C. Jeong, Phys. Rev. C **63**, 044610 (2001).

[2] V. S. Ramamurthy and S. S. Kapoor, Phys. Rev. Lett. **54**, 178 (1985).

[3] V. S. Ramamurthy, S. S. Kapoor, R. K. Choudhury, A. Saxena, D. M. Nadkarni, A. K. Mohanty, B. K. Nayak, S. V. Sastry, S. Kailas, A. Chatterjee, P. Singh, and A. Navin, Phys. Rev. Lett. **65**, 25 (1990).

[4] K. U. L. Businaro and S. Gallone, Nuovo Cimento **5**, 315 (1957); K. T. R. Davies and A. J. Sierk, Phys. Rev. C **31**, 915 (1985).

[5] D. Vorkapic and B. Ivanisevic, Phys. Rev. C **52**, 1980 (1995).

[6] R. Tripathi, K. Sudarshan, S. Sodaye, S. K. Sharma, and A. V. R. Reddy, Phys. Rev. C **75**, 024609 (2007).

[7] R. K. Gupta, M. Balasubramaniam, R. Kumar, D. Singh, S. K. Arun, and W. Greiner, J. Phys. G: Nucl. Part. Phys. **32**, 345 (2006).

[8] S. S. Malik and R. K. Gupta, Phys. Rev. C **39**, 1992 (1989).

[9] R. K. Gupta, S. K. Arun, R. Kumar, and Niyti, Int. Rev. Phys. (IREPHY) **2**, 369 (2008).

[10] R. K. Gupta, M. Balasubramaniam, R. Kumar, N. Singh, M. Manhas, and W. Greiner, J. Phys. G: Nucl. Part. Phys. **31**, 631 (2005).

[11] B. B. Singh, M. K. Sharma, and R. K. Gupta, Phys. Rev. C **77**, 054613 (2008).

[12] Niyti, R. K. Gupta and W. Greiner, J. Phys. G: Nucl. Part. Phys. **37**, 115103 (2010); R. K. Gupta, Niyti, M. Manhas and W. Greiner, *ibid.* **36**, 115105 (2009).

[13] S. Kanwar, M. K. Sharma, B. B. Singh, R. K. Gupta, and W. Greiner, Int. J. Mod. Phys. E **18**, 1453 (2009).

[14] B. B. Singh, M. K. Sharma, R. K. Gupta, and W. Greiner, Int. J. Mod. Phys. E **15**, 699 (2006).

[15] M. Balasubramaniam, R. Kumar, R. K. Gupta, C. Beck, and W. Scheid, J. Phys. G: Nucl. Part. Phys. **29**, 2703 (2003).

[16] M. K. Sharma, S. Kanwar, G. Sawhney, R. K. Gupta, and W. Greiner, J. Phys. G: Nucl. Part. Phys. **38**, 055104 (2011); D. Jain, R. Kumar, M. K. Sharma, and R. K. Gupta, Phys. Rev. C **85**, 024615 (2012).

[17] M. K. Sharma, G. Sawhney, R. K. Gupta, and W. Greiner, J. Phys. G: Nucl. Part. Phys. **38**, 105101 (2011); M. K. Sharma, G. Sawhney, S. Kanwar, and R. K. Gupta, Mod. Phys. Lett. A **25**, 2022 (2010).

[18] M. Kaur, R. Kumar, and M. K. Sharma, Phys. Rev. C **85**, 014609 (2012).

[19] K. Sandhu, M. K. Sharma, and R. K. Gupta, Phys. Rev. C **85**, 024604 (2012).

[20] P. Moller, J. R. Nix, W. D. Myers, and W. J. Swiatecki, At. Data Nucl. Data Tables **59**, 185 (1995).

[21] R. G. Stokstad, Y. Eisen, S. Kaplanis, D. Pelte, U. Smilansky, and I. Tserruya, Phys. Rev. Lett. **41**, 465 (1978).

[22] R. K. Gupta, M. Manhas, and W. Greiner, Phys. Rev. C **73**, 054307 (2006).

[23] J. E. Gindler, K. F. Flynn, L. E. Glendenin, and R. K. Sjoblom, Phys. Rev. C **16**, 1483 (1977).

[24] H. J. Lustig, J. A. Maruhn, and W. Greiner, J. Phys. G: Nucl. Part. Phys. **6**, L25 (1980).

[25] R. Vandenbosch and J. R. Huizenga, *Nuclear Fission* (New York, Academic, 1973).

[26] J. Maruhn and W. Greiner, Z. Phys. **251**, 431 (1972); R. K. Gupta, W. Scheid, and W. Greiner, Phys. Rev. Lett. **35**, 353 (1975).

[27] R. K. Gupta and W. Greiner, in *Heavy Elements and Related New Phenomena*, edited by W. Greiner and R. K. Gupta, Vol. I (World Scientific, Singapore, 1999).

[28] R. K. Gupta, M. K. Sharma, S. Singh, R. Nouicer, and C. Beck, Phys. Rev. C **56**, 3242 (1997); R. K. Gupta, M. K. Sharma, N. V. Antonenko, and W. Scheid, J. Phys. G: Nucl. Part. Phys. **25**, L47 (1999); M. K. Sharma, R. K. Gupta, and W. Scheid, *ibid.* **26**, L45 (2000).

[29] B. B. Singh, M. K. Sharma, R. K. Gupta, and W. Greiner, Int. J. Mod. Phys. E **15**, 699 (2006).

[30] H. Kröger and W. Scheid, J. Phys. G: Nucl. Part. Phys **6**, L85 (1980).

[31] J. Maruhn and W. Greiner, Phys. Rev. Lett. **32**, 548 (1974).

[32] R. K. Gupta, W. Scheid, and W. Greiner, Phys. Rev. Lett. **35**, 353 (1975).

[33] N. J. Davidson, S. S. Hsiao, J. Markram, H. G. Miller, and Y. Tzeng, Nucl. Phys. A **570**, 61C (1994).

[34] W. Myers and W. J. Swiatecki, Nucl. Phys. **81**, 1 (1966).

[35] A. S. Jensen and J. Damgaard, Nucl. Phys. A **203**, 578 (1973).

[36] R. K. Gupta, N. Singh, and M. Manhas, Phys. Rev. C **70**, 034608 (2004).

[37] M. Muenchow and W. Scheid, Phys. Lett. B **162**, 265 (1985); Nucl. Phys. A **468**, 59 (1987).

[38] M. Rashdan, A. Faessler, and W. Waida, J. Phys. G: Nucl. Part. Phys. **17**, 1401 (1991).

[39] T. Cooper, W. Bertozzi, J. Heisenberg, S. Kowalski, W. Turchinetz, C. Williamson, L. Cardman, S. Fivozinsky, J. Lightbody, Jr., and S. Penner, Phys. Rev. C **13**, 1083 (1976).

[40] S. Kumar and R. K. Gupta, Phys. Rev. C **55**, 218 (1997).

[41] H. S. Khosla, S. S. Malik, and R. K. Gupta, Nucl. Phys. A **513**, 115 (1990).

[42] R. K. Gupta, S. Kumar, and W. Scheid, Int. J. Mod. Phys. E **6**, 259 (1997).

[43] T. Matsuse, C. Beck, R. Nouicer, and D. Mahboub, Phys. Rev. C **55**, 1380 (1997).

[44] S. J. Sanders, Phys. Rev. C **44**, 2676 (1991).

[45] S. J. Sanders, D. G. Kovar, B. B. Back, C. Beck, D. J. Henderson, R. V. F. Janssens, T. F. Wang, and B. D. Wilkins, Phys. Rev. C **40**, 2091 (1989).

[46] G. Royer and J. Mignen, J. Phys. G: Nucl. Part. Phys. **18**, 1781 (1992).

[47] A. J. Sierk, Phys. Rev. C **33**, 2039 (1986).

[48] S. K. Arun, R. Kumar, and R. K. Gupta, J. Phys. G: Nucl. Part. Phys. **36**, 085105 (2009).